Reaction of Carbon Dioxide Gas Absorption with Suspension of Calcium Hydroxide in Slurry Reactor

Zahrul Mufrodi [1*], L. M. Shitophyta [1], Hary Sulistyo [2], Rochmadi [2], Muhammad Aziz [3]

[1] Department of Chemical Engineering, Faculty of Industrial Technology, Achmad Dahlan University, Yogyakarta, 55191, Indonesia.

[2] Department of Chemical Engineering, Gadjah Mada University, Jl. Grafika No. 2, Bulaksumur, Yogyakarta 55281, Indonesia.

[3] Institute of Industrial Science, University of Tokyo, 4-6-1 Komaba, Meguro-ku, Tokyo 153-8505, Japan.

Abstract

Chemical phenomena involving three phases (solid, liquid, and gas) are often found in the industry. Carbonate ($CaCO_3$) is widely used in industries as a powder-making material in the cosmetic industry, a pigment in the paint industry, and filler in the paper and rubber industry. This research aim to study the ordering process carbonate deposits ($CaCO_3$) from the absorption process of CO_2 gas with $Ca(OH)_2$ suspension. The absorption reaction of CO_2 gas with $Ca(OH)_2$ suspension was carried out in a stirred slurry tank reactor. Initially, the reactor containing water was heated to a certain temperature, then $Ca(OH)_2$ was added to the reactor. Furthermore, CO_2 gas with a certain flow rate and temperature (according to the reactor temperature) is flown with the help of a gas distributor. Samples were taken every 1 min until the concentration of $Ca(OH)_2$ could not be detected (completely reacted). The variables in this study were: stirrer rotation speed (5.667–11.067 rps), CO_2 gas flow rate (34.0127–60.5503 c/s), and temperature (30–50°C). The mass transfer coefficient and the reaction rate coefficient were determined by minimizing Sum of Squares of Errors (SSE). This experimental process follows a dynamic regime. A dimensionless number relationship for the gas-liquid mass transfer for the value range is $Re_l = 18928.76$–38217.20, $Sh = 0.07928\ Re_g^{0.4383}\ Re_l^{0.4399}\ Sc^{0.6415}$ with an error of 5.19%. The dimensionless number relationship for solid-liquid mass transfer is $Sh = 0.0001179\ Re_g^{0.4674}\ Re_l^{0.5403}\ Sc^{1.444}$ with an error of 7.31%. The relationship between the reaction rate constant and the temperature in the 30-50 °C range can be approximated by the Arrhenius equation, namely $k_r = 1771000\ e^{-2321.4/T}$ cm³/mgmol/s with an error of 3.63%.

1- Introduction

$CaCO_3$ is one of the most plentiful biomaterials. It is not only used as an essential building material in the organism but also as a filler in paints, plastics, rubber, and paper [1]. $CaCO_3$ has a polymorphic structure with three crystal phases: aragonite, calcite, and vaterite [2]. Calcite is the most constant phase at room temperature and atmospheric conditions, whereas aragonite and vaterite are metastable polymorphs that immediately convert into calcite [3]. $CaCO_3$ of the calcite structure can be synthesized by the reaction of CaO and CO_2 under a wide range of conditions. During the calcite synthesis through the reaction of CaO and CO_2, a thin layer of $CaCO_3$ appears first on the CaO solid-grain surface [4].

Chemical phenomena involve three phases (solid, liquid, and gas) and are widely applied in industry, including the carbonation and sulfidation processes in sugar factories and the production of ammonium sulfate, ammonium hydroxide, and carbon dioxide. Another process that involves a three-phase system is calcium carbonate ($CaCO_3$) production.

---

* **CONTACT**: zahrul.mufrodi@che.uad.ac.id

$CaCO_3$ is mainly used as a filler material in paint, plastic, paper, food, ceramics, medicine, and other industries [5]. It is widely found in nature in the form of limestone; however, due to its low purity, the level of refinement is not sufficient for use in industries.

$CaCO_3$ preparation can be done by a three-phase reaction using a stirred slurry tank reactor. Compared to other three-phase reactors, the stirred slurry tank reactor has several advantages, such as simple construction and design, good heat transfer performance, online catalyst addition and removal, and equitable interphase mass transfer rates with low energy input [6]. Calcium-based sorbents for adsorption of CO_2 are significant matter due to their potential variety of application fields to decrease CO_2 greenhouse gas and have been improved with diverse structures and compositions to enhance the adsorption capacity [7]. Many previous studies have focused on the synthesis of $CaCO_3$ through the reaction of carbon dioxide and calcium hydroxide. Jin et al. [8] studied the effect of ethanolamine concentration, reaction temperature, reaction pressure, and reaction time on the polymorphs of $CaCO_3$. Liendo et al. [9] investigated the effect of gas flow rate and initial CaCO on the synthesis of $CaCO_3$ through the carbonation route in a continuously Stirred Bubble Reactor and a Packed Bed Reactor Shirsath et al. [10] investigated the effect of $Ca(OH)_2$ slurry concentration, CO_2 flow rate, $Ca(OH)_2$ slurry flow rate on the particle size and morphology of $CaCO_3$. Made et al. [11] studied the production of $CaCO_3$ from natural CaO into nano-sizes with varying concentrations of $Ca(OH)_2$. Kamba et al. [12] synthesized pure $CaCO_3$ nanocrystals using a high-pressure homogenizer (HPH). The reaction CO_2 and slurry of $Ca(OH)_2$ was controlled by diffusion and reaction in the low temperature range and controlled by diffusion in the high temperature range [13]. However, no study has investigated the correlation of dimensionless numbers on gas-liquid mass transfer coefficients from the manufacturing of $CaCO_3$. Therefore, this study aims to determine mass transfer, coefficients, rate constants, and dimensionless numbers from the production of precipitated $CaCO_3$ by CO_2 absorption using $Ca(OH)_2$.

2- Material and Methods

2-1- Material Preparation

CO_2 with a purity of 99.98% was obtained from PT. Samator Gas Industry, Yogyakarta, Indonesia. $Ca(OH)_2$ having purity of 96% and an average grain size of 0.0005 cm was obtained from UD Organic, Yogyakarta, Indonesia.

2-2- CaCO₃ Production

A tank with a width of 1 cm and an inner diameter of 12.64 cm which was equipped with four baffles was used as a reactor. A pitched blade turbine with a diameter of 5.34 cm was used as a stirrer. The used gas distributor was in the form of a pipe ring with a diameter of 7.8 cm and a hole distance of 0.5 cm. A diagram of experimental instruments is presented in Figure 1.
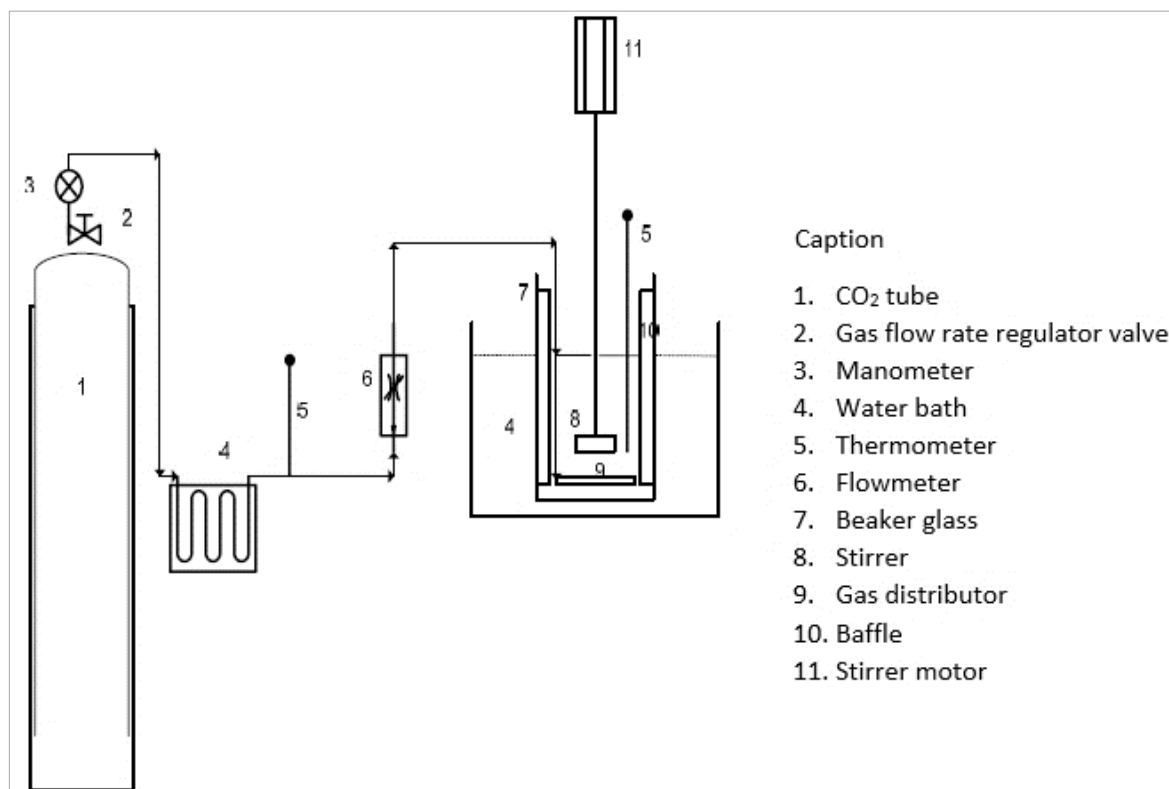
Figure 1. A scheme of experimental setup using a stirred tank reactor

The reactor tank was filled with 2 L of distilled water, then it was heated at a temperature of 30-50 °C. The water bath which was passed by the CO_2 gas pipe was heated so that the gas flow temperature was the same as the reactor temperature. 10 g of $Ca(OH)_2$ was fed into the reactor. The stirrer was varying at rotation rates of 5.667 rps to 1.067 rps to form a saturated solution of $Ca(OH)_2$. The gas valve was opened at flow rate variation of 34.0127 cm/s to 60.5503 cm/s and inflated in the reactor with the help of a gas distributor. In every 1 min, the sample was taken to analyze the remaining $Ca(OH)_2$ concentration. The experiment was stopped after the $Ca(OH)_2$ content had finished reacting which was indicated by the colour of the sample that did not change to pink when the phenolphthalein (PP) indicator was dropped.

3- Result and Discussion

3-1- Effect of Stirrer Speed

Experiments were carried out by varying the stirring speed, CO_2 flow rate (C_A), and temperature towards the changes of $Ca(OH)_2$ concentration (C_B) in the reactor during the reaction. The stirring speed was varied by observing visually during the experiment the homogeneity of the solution and the presence of vortices. The rate of gas flow cogitated the rate of absorption of the liquid against the gas, while the temperature was started from the ambient temperature with an interval of 5 °C. Sampling every 1 min was the fastest time that allows sampling and detection of the presence of $Ca(OH)_2$ in the sample.

The stirrer speed varied from 5.667 to 1.067 rps, while other variables were kept constant. In this process, the greater stirring reduced the mass transfer barrier of $Ca(OH)_2$ to water which led to more reacted $Ca(OH)_2$. Besides, the increase in stirring rate would enhance the interfacial area, therefore, the $Ca(OH)_2$ dispersion in water becomes more complete. This phenomenon is consentient with the previous result conducted by [9] who stated that the low stirring speed led to the low mass transfer, while the high stirring rate accelerated the mass transfer rate.

Figure 2 shows the correlation between the $Ca(OH)_2$ concentration with the time at different stirring speeds. It indicates that the longer the stirring would decrease the concentration of $Ca(OH)_2$ in the solution. If the stirring rate was increased for the same period, the decrease in the concentration of $Ca(OH)_2$ would also increase. The largest decrease in the rate occurred at the highest stirring speed of 9.467 rps. This phenomenon is consentient to the previous result conducted by Fan et al. [14] who stated that the low stirring speed led to the low mass transfer, while the high stirring rate accelerated the mass transfer rate. The values of liquid-gas mass transfer coefficient (k_la_g) and solid-liquid mass transfer coefficient (k_s) on the variation of stirring speed were calculated using the Hooke-Jeeves method. The relationship between the stirring rate and the k_la_g and k_s variables is shown in Figure 3.
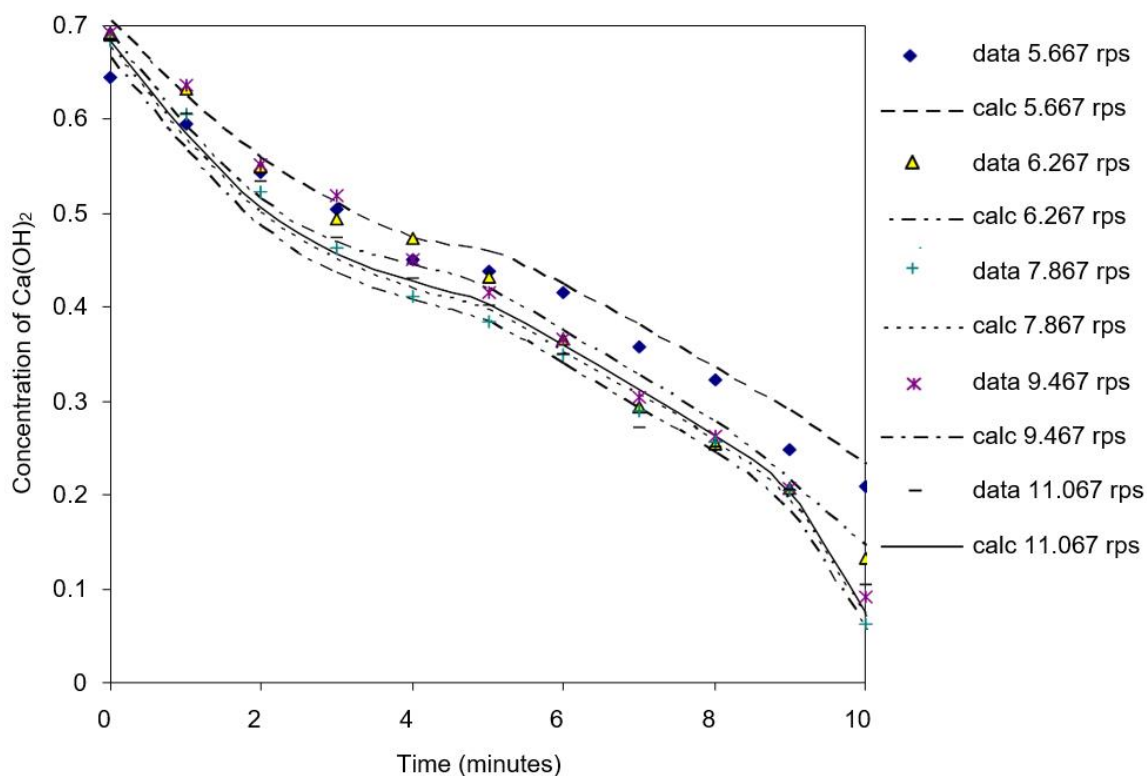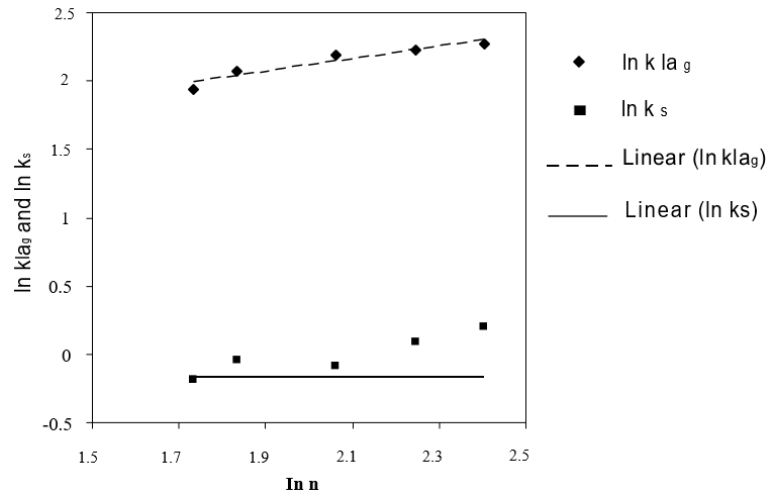

Figure 2. The relationship between the concentration of Ca(OH)₂ with time at a various stirring speed

Figure 3. The relationship between ln k_la_g and ln k_s with ln N

The equations that represent the relationship in Figure 3 are:

$$k_la_g = 3.3198 \, N^{0.456} \tag{1}$$

$$k_s = 2.7988 \, N^{0.4972} \tag{2}$$

The approximation errors of Equations 1 and 2 were 3.41% and 4.39%, respectively.

The value of the k_la_g increased by the increase of stirring. This phenomenon shows that higher stirring speed leads to the smaller mass transfer barrier of CO_2 gas into the water, as a result, higher k_la_g and larger amount of CO_2 diffused into the water can be obtained. Babou et al. [15] stated that increasing the stirrer speed resulted in a reduction of particle size. The decrease in the particle size with the increase in stirring speed can expand the formation of the huge number of small nuclei, thus, generating much larger particles.

3-2- The Effect of CO$_2$ Gas Flow Rates

Flowrate varied from 34.0127 to 60.5503 cm/s to determine the effect of CO_2 flow rate. Increasing the flow rate of CO_2 would accelerate the reduction of $Ca(OH)_2$, especially for the rates between 9.925–11.883 mL/s. The correlation of the concentration of $Ca(OH)_2$ at various CO_2 gas flow rates, including both the experimental data and calculation is shown in Figure 4.
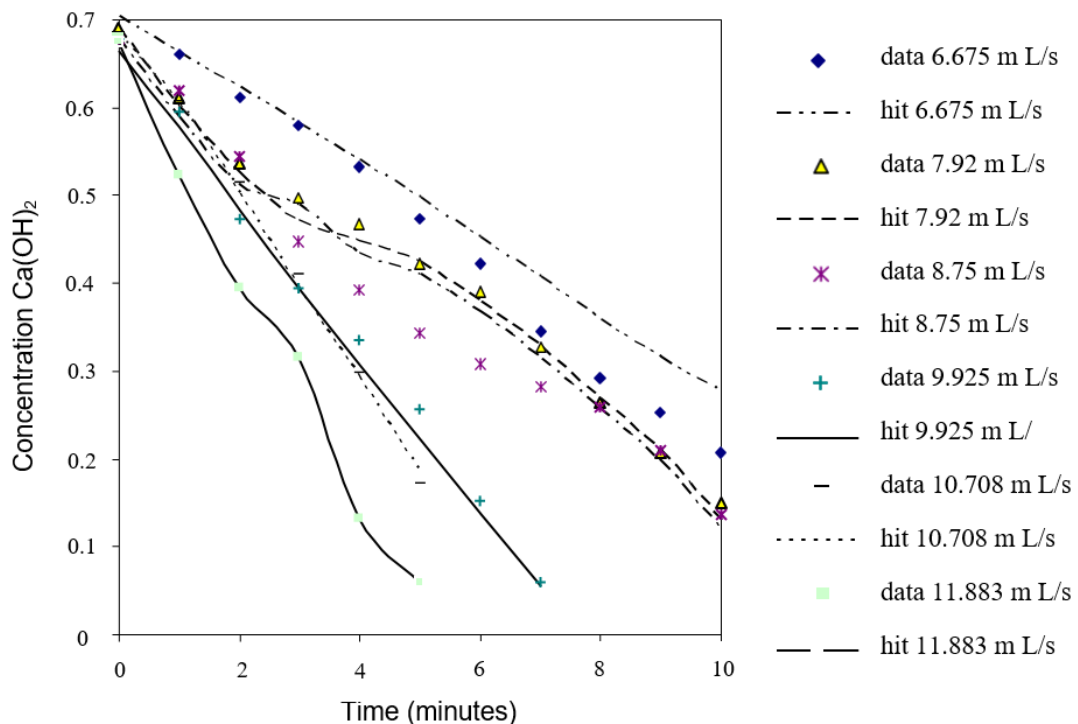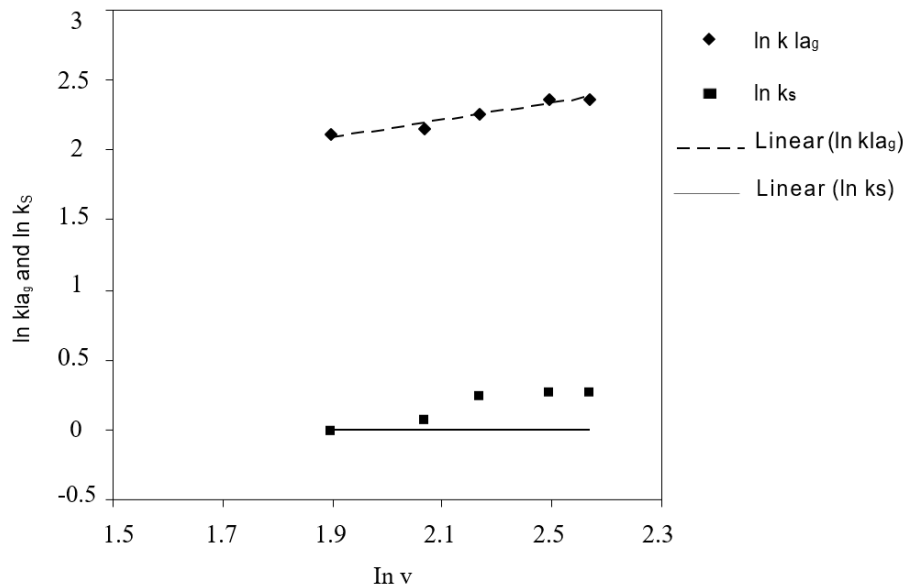

Figure 4. The relationship between the concentration of Ca(OH)$_2$ in mgmol/cm^3 with time at various gas flow rates

Figure 4 shows that the higher the gas flow rate, the concentration of $Ca(OH)_2$ reduced faster. The result indicates that a higher gas flow rate leads to the larger swelling of the CO_2 gas which diffuses as carbonic acid (H_2CO_3), then carbonic acid will be broken down into H+ and $CO_3^=$ and reacted with the dissolved $Ca(OH)_2$. A lower CO_2 flow rate with conventional stirring may give a beneficial state for the formation of plate-like particles [10, 16]. CO_2 gas flow rate also affects reaction time, percentage phase, and crystal size. Increasing CO_2 gas flow rate decreases the particle size [17].

The concentration of $Ca(OH)_2$ in the simulation was close to the experimental data with an average error ranging 0.12-8.84%. This result proved that the process can be approached by existing mathematical models. The relationship between k_la_g and k_s on changes in the flow rate of CO_2 gas can be seen in Figure 5.

Figure 5. The relationship between ln k_la_g and ln k_s with ln N

The equations that represent Figure 5 are:

$$k_la_g = 0.9616 \ v^{0.6028} \tag{3}$$

$$k_s = 0.8744 \ v^{0.6244} \tag{4}$$

with the approximation error of Equations 3 and 4 were 2.22% and 7.79%, respectively.

The enlarged gas flow rate of CO_2 would increase the dissolution turbulence hence, it would have the same tendency (pattern) as the change in the stirring speed.

3-3- Effect of Changes in Reaction Temperature

The effect of the reaction temperature was carried out at temperature of 30-50°C, while other variables were kept constant. At 35°C, the concentration of $Ca(OH)_2$ was lower than the one at the temperature of 30 °C. After that, the $Ca(OH)_2$ concentration enhanced with an increase in temperature. This phenomenon occurred because, at temperatures between 30–35°C, the reaction equilibrium has reached. The increase in temperature decreased the formation of $CaCO_3$ [18].

As shown in Figure 6, temperature affected the reaction rate. Temperature changes affected the decrease of the concentration of $Ca(OH)_2$ in the solution. Temperature increase had a relatively smaller effect on reducing $Ca(OH)_2$ concentration than the stirring speed and the CO_2 gas flow rate. This case happened because the higher the temperature, the smaller the amount of solid $Ca(OH)_2$ and CO_2 gas dissolved in the water. Temperature increase can increase the particle size which can be described by the competition existing between the nucleation and crystalline growth phases. At low temperatures, the nucleation rate is greater than the crystalline growth, thus, generating small particles sizes. On the contrary, the high temperature produces the larger particle sizes [15].
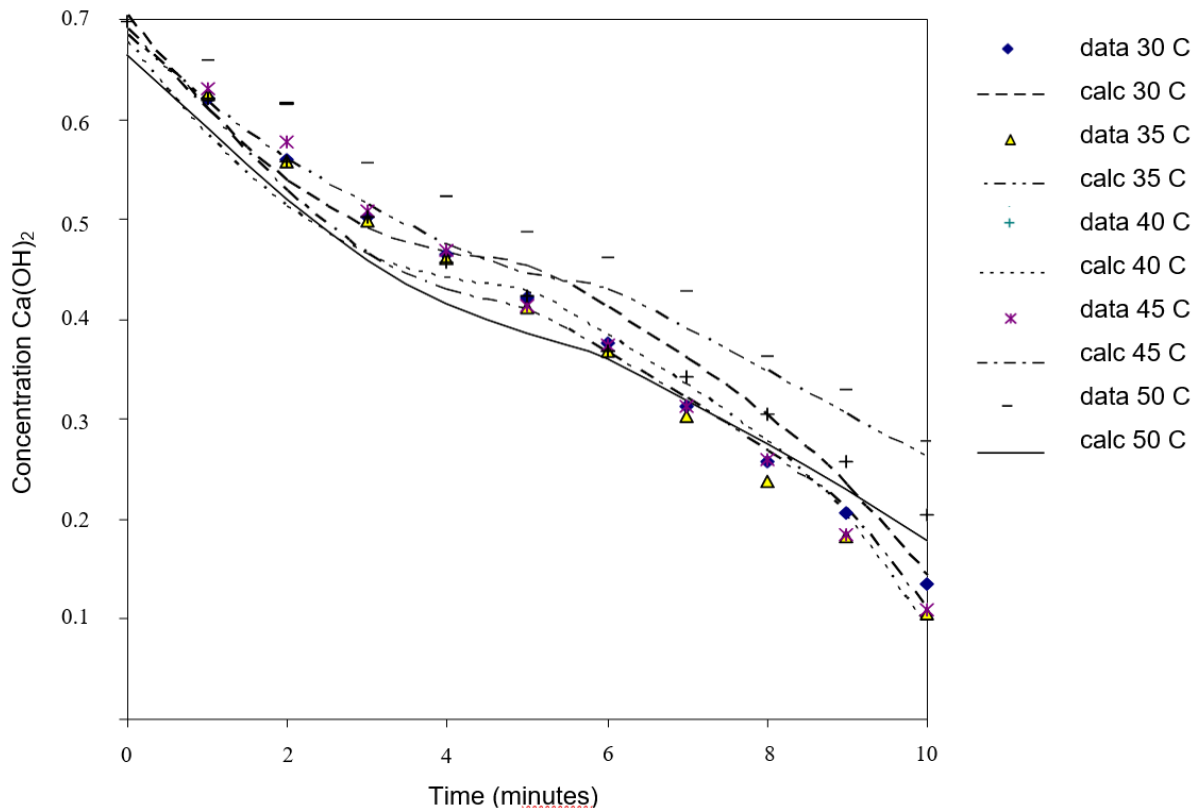
Figure 6. The relationship between the concentration of Ca(OH)$_2$ mgmol/cm^3 with time at various temperatures

The optimization results of the reaction rate constants at various temperatures can be seen in Table 1.

Table 1. Optimization of k$_r$ at various temperatures

Temperature (ºC)	k$_r$ (cm^3/mgmol·s)
30	836.69
35	947.39
40	1068.48
45	1200.50
50	1343.98

Equation 5 expresses the relationship between the constant rate of reaction and temperature in the Arrhenius equation:

$$k_r = 1.771 \times 106 \, e^{-2321.4/T} \, cm^3/mgmol/s \qquad 5$$

with a mean error of 3.63%.

The ratios of the reaction rate constant for the difference in temperature increase of 10°C were: 1.277 (3040°C), 1.2672 (35-45°C), and 1.2578 (40-50°C). The results showed that the rate constant ratios were less than 1.5 at the temperature difference of 10°C.

Johnstone & Thring [19] stated that if the ten degrees coefficient (Q$_{10}$) is greater than 2, then the characteristic is classified as a chemical regime. However, if Q$_{10}$ is below 1.5, the character is considered as a dynamic regime. Q$_{10}$ value obtained in this study is less than 1.5, therefore, the characters in this study are included as a dynamic regime. In this regime, the reaction rate is affected by the mass transfer rate and depends on the fluid flow velocity. The reaction rate is also affected by the speed of stirring.

If the mass transfer rate of CO$_2$ from gas to liquid and the dissolution of Ca(OH)$_2$ was considered to be the same as the reaction rate, the overall reaction rate constant is:

$$\frac{1}{k_0} = \frac{1}{k_1 a_g} \frac{P_A}{H C_B^* . k_s a_s} + \frac{1}{k_r C_B^*} - \frac{r_c}{k_s a_s . k_g a_g C_B^*} \qquad (6)$$

When viewed from the existing resistance, the changes can be seen in Table 2.

Table 2. Resistances which affect variables

Variables		Resistances		
		$1/k_l a_g$	$P_A/HC_B^* k_s a_s$	$1/k_r C_B^*$
v_g (cm/s)	34.0127	0.1241	6.7061×10^{-08}	0.0388
	40.3567	0.1119	6.0269×10^{-08}	0.0424
	44.5860	0.1054	5.6633×10^{-08}	0.0446
	50.5732	0.0977	5.2348×10^{-08}	0.0476
	54.5631	0.0933	4.9924×10^{-08}	0.0495
N (rps)	5.667	0.1366	7.8749×10^{-08}	0.0356
	6.267	0.1305	7.4906×10^{-08}	0.0369
	7.867	0.1241	6.7061×10^{-08}	0.0388
	9.467	0.1082	6.1016×10^{-08}	0.0432
	11.067	0.1007	5.6458×10^{-08}	0.0459
Temperature (K)	303.15	0.1241	6.7061×10^{-08}	0.0388
	308.15	0.1036	6.9952×10^{-08}	0.0406
	313.15	0.1013	5.4006×10^{-08}	0.0458
	318.15	0.0992	4.2160×10^{-08}	0.0515
	323.15	0.0972	3.3464×10^{-08}	0.0576

As shown in Table 2, the dominant regime for this experiment is the gas-liquid mass transfer regime, which can be seen from the overall reaction rate constant. The value of $1/k_l a_g$ was greater than the values of $P_A/(HC_B^* k_s a_s)$ and $1/(k_r C_B^*)$. Although the resistance to gas-liquid mass transfer is the most influential parameter, however, the magnitude of the resistance to the reaction rate cannot be neglected because its value was only half of the gas-liquid mass transfer resistance.

3-4- The Relationship between the Dimensionless Number at Various Gas-liquid Mass Transfer Coefficient

The author declares that there is no conflict of interests regarding the publication of this manuscript. In addition, the ethical issues, including plagiarism, informed consent, misconduct, data fabrication and/or falsification, double publication and/or submission, and redundancies have been completely observed by the authors.

The mass transfer rate from gas to liquid is affected by many factors, such as bubble diameter, gas flow rate, liquid physical properties, and stirring speed. This effect can be reflected by the relationship between Sherwoods number (Sh), gas Reynolds number (Re_g), liquid Reynold's number (Re_l), and Schmidt's number (Sc). The number relationship approach was carried out by an analysis of dimensionless number which results in Equation 7.

$$Sh = 0.07928\, Re_g^{0.4383}\, Re_l^{0.4399}\, Sc^{0.6415} \tag{7}$$

with an average error of 5.19%.

Equation 7 shows that the higher the Re_l the faster the stirring will increase the Sh. This is due to the phenomenon that faster stirring cycle results in the smaller mass transfer barrier of CO_2 gas into the water. Therefore, $k_l a_g$ increases, which finally enhances the amount of CO_2 diffused into the water. Larger amount of CO_2 gas that diffuses into the water leads to larger formation of H_2CO_3

Re_g increases following the increase of CO_2 gas flow rate acceleration that causes the increase of solution turbulence. As the result, a same pattern with the change of stirring speed was obtained. However, the effect of the change in stirring is slightly greater than the increase in flow velocity on the cla_g value $k_l a_g$.

Reduction of Sc will decrease the Sh. An increase of the temperature change would increase the coefficient of gas diffusivity in the liquid y(D) and decrease the Sc because Sc is inversely proportional to the temperature. The relationship between Sh, Re_g, Re_l, and Sc on various cla_g values are presented in Table 3.

Table 3. Relationship between Sherwood's number (both experimental data and calculation), Re, Rel, and Schmidt's number on various clag values

Variables		$k_l a_g$	Sh (data)	Sh (calc.)	Re_g	Re_l	Sc
v_g (cm/s)	34.0127	8.1999	5324.653	5513.598	398.408	26277.14	554.3612
	40.3567	8.58	5571.442	5942.776	472.7178	26277.14	554.3612
	44.586	9.5599	6207.791	6208.122	522.2577	26277.14	554.3612
	50.5732	10.55	6850.662	6560.623	592.3894	26277.14	554.3612
	54.5631	10.55	6850.662	6782.648	639.1241	26277.14	554.3612
	5.667	6.9399	4506.462	4773.377	398.408	18928.76	554.3612
	6.267	7.9	5129.873	4989.244	398.408	20932.86	554.3612
N (rps)	7.867	8.947	5809.741	5513.598	398.408	26277.14	554.3612
	9.467	9.28	6025.977	5980.98	398.408	31621.42	554.3612
	11.067	9.61	6240.268	6405.87	398.408	36965.7	554.3612
Temperature (K)	303.15	10.18	6610.396	5513.595	398.4076	26277.14	554.3612
	308.15	10.18	5884.399	5268.67	450.7962	29732.45	436.1288
	313.15	9.94	5461.542	5181.605	482.113	31797.97	387.6331
	318.15	9.61	5139.044	5237.945	543.2229	35828.5	334.8277
	323.15	9.4199	4806.119	5160.462	579.4398	38217.2	299.4861

The power of Re at a dimensionless number group equation can be used to indicate the appropriate regime. This is expressed as the Reynolds index, which was obtained from the variation of the Re at a fixed temperature. If the Reynolds index value is close to zero, it includes a viscous chemical or dynamic regime. If the value is between 0.5 and 0.8, it is called a turbulent dynamic regime for the fixed interface. If the index is between 3 and 5, the characteristic is the dynamic regime for the free interface [20]. When following these limitations, as the process has a Reynolds index close to 0.5, therefore, it can be included in the dynamic regime category for the free interface. This is following the review regime based on Q_{10} which states that this process is a dynamic regime.

3-5- The Relationship between the Dimensionless Number at Various Solid-liquid Mass Transfer Coefficient

The solid-liquid mass transfer coefficient as reflected in the change in Sh as a function of the Re_g, Re_l, and Sc is shown in Equation 8;

$$Sh = 0.0001179\, Re_g^{0.4674} Re_l^{0.5403}\, Sc^{1.444} \tag{7}$$

with an average error of 7.31%.

The power of the Sc in this experiment was 1.444. According to the literature that the rank of the Sc is less than 1. This difference may be caused by the factors that affect Sc which is not measured directly (experimental variable) but from the literature review. The values of Equation 8 on various ks data is shown in Table 4.

Table 4. Relationship between Sh (experimental data and calculation), Re_g, Re_l, and Sc on various k_s values

Variables		k_s	Sh(data)	Sh(calc.)	Re_g	Re_l	Sc
v_g (cm/s)	34.0127	0.99	0.1575	0.1683	1.992	26277.14	2.7162
	40.3567	1.06	0.1686	0.1823	2.3635	26277.14	2.7162
	44.586	1.2599	0.2004	0.191	2.6112	26277.14	2.7162
	50.5732	1.2899	0.2052	0.2026	2.9619	26277.14	2.7162
	54.5631	1.2899	0.2052	0.2099	3.1956	26277.14	2.7162
N (rps)	5.667	0.831	0.1322	0.1409	1.992	18928.76	2.7162
	6.267	0.9601	0.1527	0.1488	1.992	20932.86	2.7162
	7.867	0.9101	0.1448	0.1683	1.992	26277.14	2.7162
	9.467	1.091	0.1736	0.186	1.992	31621.42	2.7162
	11.067	1.221	0.1942	0.2024	1.992	36965.7	2.7162
Temperature (K)	303.15	1.1699	0.1862	0.1683	1.992	26277.14	2.7162
	308.15	1.14	0.1681	0.1429	2.2539	29732.45	2.2256
	313.15	0.97	0.1351	0.1278	2.4105	31797.97	1.9651
	318.15	0.75	0.0995	0.113	2.7161	35828.5	1.6608
	323.15	0.75	0.0957	0.1038	2.8971	38217.2	1.4974

The change in the increase of the Reynolds number of liquid was indicated by an increase in the stirring speed which would increase the Sherwood number. The increase in stirring speed facilitates the breakdown of $Ca(OH)_2$ into Ca^{++} and $OH^=$ The dispersed Ca^{2+} in the water increased resulting in an increase of the k_s. The same thing will happen in the increase of the Reynolds number of gas with an increasing flow rate of CO_2 gas. Increasing the temperature change will result in a higher and a decrease in the Sc because Sc is inversely proportional to the diffusivity. A decrease in temperature will decrease the k_s.

From the calculation, the Reynold index is 0.6. The index is between 0.5 and 0.8, therefore, this process has dynamic regime characteristics for fixed interfaces. These results are consistent with the review of gas-liquid mass transfer coefficients, which categorize this process as a dynamic regime for the fixed interface.

The rate constant in this study is almost the same with the previous research conducted by Fernianti [21] regarding the reaction of solid CO_2 and $CaCO_3$ gas in a stirred tank slurry reactor at a temperature range of 2045°C, namely $k_{r1} = 1.47 \times 10^6 e^{-2290/T}$ cm^3/mgmol·s and $k_{r2} = 1767.75$ $e^{-2021.35/T}$ s^{-1}.

In the previous research conducted by Vasconceles et al. [20] stated that the gas-liquid mass transfer analysis for high Re in the bubble reactor has Reynold's power, namely: $Sh = 1.13$ $Re^{1/2}Sc^{1/2}$, whereas, the boundary layer theory for laminar velocity follows the Froessling equation for the solid form $Sh = c$ $Re^{1/2}Sc^{1/3}$. The c value is close to 0.6 or other experiments get a value between 0.42 and 0.95.

In the gas-liquid reaction experiment with a solid catalyst, the reaction takes place quickly with a Re_l was greater than 25, hence, the solid-liquid mass transfer coefficient equation is as follows [22].

$$k_s = 0.6 \ (D_A/d_p) \ Re_l^{1/2} \ Sc^{1/3} \tag{9}$$

When compared with this process, it turns out that the Reynold index has almost the same value as the equation above and belongs to the same regime, namely the dynamic regime for the fixed interface. This means that the experimental results have the same trend as the previous experiment.

4- Conclusion

This experiment was carried out to explore the effect of stirring speed, CO_2 flow rate, and temperature on the synthesis of $CaCO_3$ during the reaction of CO_2 and $Ca(OH)_2$. Increasing stirring speed decreased the concentration of $Ca(OH)_2$. thus, the formation of $CaCO_3$ also gets dropped. Reduction of $Ca(OH)_2$ concentration occurs faster as rising of CO_2 flow rate. The increase in temperature lowers the formation of $CaCO_3$. A mathematical model can be applied to the experimental process, as proved by simulations that approach experimental data. This experimental process follows a dynamic regime. A dimensionless number relationship for the gas-liquid mass transfer for the value range $Re_l = 18928.76-38217.20$, $Sh = 0.07928$ $Re_g^{0.4383}$ $Re_l^{0.4399}$ $Sc^{0.6415}$ with an error of 5.19%. The dimensionless number relationship for solid-liquid mass transfer is $Sh = 0.0001179$ $Re_g^{0.4674}$ $Re_l^{0.5403}$ $Sc^{1.444}$ with an error of 7.31%. The relationship between the reaction rate constant and the temperature in the 30–50 °C range can be approximated by the Arrhenius equation, namely, $k_r = 1771000$ $e^{-2321.4/T}$ cm^3/mgmol·s with an error of 3.63%.

5- Nomenclature

a_g	Area of boundary gas-liquid per unit volume of liquid, cm^2/cm^3	a_s	Area of boundary solid-liquid per unit volume of liquid, cm^2/cm^3
C_B^*	Concentration of $Ca(OH)_2$, mgmol/cm^3	D_A	Coefficient of gas diffusivity in the liquid, cm^2/s
d_p	Particle diameter, cm	H	Henry's constant
k_la_g	Liquid-gas mass transfer coefficient, cm/s	k_r	Reaction rate constants, cm^3/mgmol.s
k_s	Solid-liquid mass transfer coefficient, cm/s	N	Stirrer rotation speed, rps
P_A	CO_2 gas pressure, atm	Re	Reynolds number
Re_g	Gas Reynolds number	Re_l	Liquid Reynolds number
Sc	Schmidt number	Sh	Sherwood number
v_g	Gas flowrate, cm/s		

6- Declarations

6-1- Author Contributions

Conceptualization, Z.M. and R.; methodology, Z.M. and H.S.; simulation, Z.M. and R.; validation, Z.M., H.S., M.A., and R.; formal analysis, Z.M.; resources, Z.M.; data curation, Z.M.; writing—original draft preparation, Z.M.; writing—review and editing, H.S., R., L.M.S., and M.A.; visualization, L.M.S.; supervision, H.S., R., and M.A.; project administration, L.M.S.; funding acquisition, Z.M. All authors have read and agreed to the published version of the manuscript.

6-2- *Data Availability Statement*

The data presented in this study are available on request from the corresponding author.

6-3- *Funding*

The authors received no financial support for the research, authorship, and/or publication of this article.

6-4- *Institutional Review Board Statement*

Not applicable.

6-5- *Informed Consent Statement*

Not applicable. This study was not involving humans or animals.

6-6- *Conflicts of Interest*

The authors declare that there is no conflict of interest regarding the publication of this manuscript. In addition, the ethical issues, including plagiarism, informed consent, misconduct, data fabrication and/or falsification, double publication and/or submission, and redundancies have been completely observed by the authors.

7- References

[1] Ramakrishna, C., Thenepalli, T., & Ahn, J. W. (2017). A brief review of aragonite precipitated calcium carbonate (PCC) synthesis methods and its applications-. Korean Chemical Engineering Research, 55(4), 443–455. doi:10.9713/kcer.2017.55.4.443.

[2] Arifin, Z., Zainuri, M., Cahyono, Y., & Darminto. (2018). The Influence of Temperature and Gas Flow Rate on the Formation $CaCO_3$ Vaterite Phase. IOP Conference Series: Materials Science and Engineering, 395, 012004. doi10.1088/1757-899x/395/1/012004.

[3] Han, Y. S., Hadiko, G., Fuji, M., & Takahashi, M. (2005). Effect of flow rate and CO_2 content on the phase and morphology of $CaCO3$ prepared by bubbling method. Journal of Crystal Growth, 276(3–4), 541–548. doi:10.1016/j.jcrysgro.2004.11.408.

[4] Sun, Z., Luo, S., Qi, P., & Fan, L. S. (2012). Ionic diffusion through Calcite ($CaCO3$) layer during the reaction of CaO and CO2. Chemical Engineering Science, 81(1), 164–168. doi:10.1016/j.ces.2012.05.042.

[5] Erdogan, N., & Eken, H. A. (2017). Precipitated Calcium carbonate production, synthesis and properties. Physicochemical Problems of Mineral Processing, 53(1), 57–68. doi:10.5277/ppmp170105.

[6] Wang, T., Wang, J., & Jin, Y. (2007). Slurry reactors for gas-to-liquid processes: A review. Industrial and Engineering Chemistry Research, 46(18), 5824–5847. doi:10.1021/ie070330t.

[7] Kim, B. J., Park, E. H., Choi, K. D., & Kang, K. S. (2017). Synthesis of $CaCO_3$ using CO_2 at room temperature and ambient pressure. Materials Letters, 190, 45–47. doi:10.1016/j.matlet.2016.12.030.

[8] Jin, T., Tian, X., Hong, H., Zhu, N., Han, L., & Suo, Q. (2020). Study on preparation and crystalline transformation of nano- and micro-CaCO3 by supercritical carbon dioxide. Powder Technology, 370, 29–38. doi:10.1016/j.powtec.2020.05.021.

[9] Liendo, F., Arduino, M., Deorsola, F. A., & Bensaid, S. (2021). Optimization of $CaCO_3$ synthesis through the carbonation route in a packed bed reactor. Powder Technology, 377, 868–881. doi:10.1016/j.powtec.2020.09.036.

[10] Shirsath, S. R., Sonawane, S. H., Saini, D. R., & Pandit, A. B. (2015). Continuous precipitation of calcium carbonate using sonochemical reactor. Ultrasonics Sonochemistry, 24, 132–139. doi:10.1016/j.ultsonch.2014.12.003.

[11] Adnyani, N. M. L. G., Febrida, R., Karlina, E., Cahyanto, A., & Joni, I. M. (2020). Synthesis of nano calcium carbonate from natural CaO by CO_2 fine bubbling method. 3rd International Conference on Condensed Matter and Applied Physics (ICC-2019). doi:10.1063/5.0003072.

[12] Shafiu Kamba, A., Ismail, M., Tengku Ibrahim, T. A., & Zakaria, Z. A. B. (2013). Synthesis and characterisation of calcium carbonate aragonite nanocrystals from cockle shell powder (Anadara granosa). Journal of Nanomaterials, 2013, 1–10. doi:10.1155/2013/398357.

[13] Park, S. Y., & Choi, W. S. (2004). Effects of operating factors on the particle size distribution and particle shape of synthesized precipitated $CaCO_3$: Effect of reaction temperature, blowing rate of CO2 gas and initial slurry concentration of $Ca(OH)_2$ on reaction completion time. Advanced Powder Technology, 15(1), 1–12. doi:10.1163/15685520460740034.

[14] Fan, H., Song, H., Rao, Y., Wang, X., Zhu, G., Wang, Q., Qi, Y., Zhu, G., Gao, D., & Liu, J. (2019). Effect of calcium hydroxide concentration and stirring rate on the crystallization of the calcium carbonate on the surface of fly ash. BioResources, 13(3), 7017–7025. doi:10.15376/biores.13.3.7017-7025.

[15] Babou-Kammoe, R., Hamoudi, S., Larachi, F., & Belkacemi, K. (2012). Synthesis of $CaCO_3$ nanoparticles by controlled precipitation of saturated carbonate and calcium nitrate aqueous solutions. Canadian Journal of Chemical Engineering, 90(1), 26–33. doi:10.1002/cjce.20673.

[16] Gong, J., Rong, S., Wang, X., & Zhou, Y. (2022). Critical review of catalytic degradation of formaldehyde via MnO_2: From the perspective of process intensification. Journal of Cleaner Production, 134242. doi:10.1016/j.jclepro.2022.134242

[17] Munawaroh, F., Muharrami, L. K., Triwikantoro, & Arifin, Z. (2018). The effect of CO2 gas flow rate on precipitated $CaCO_3$ formed at room temperature. AIP Conference Proceedings. doi:10.1063/1.5054513.

[18] Sheng, K., Ge, H., Huang, X., Zhang, Y., Song, Y., Ge, F., Zhao, Y., & Meng, X. (2020). Formation and Inhibition of Calcium Carbonate Crystals under Cathodic Polarization Conditions. Crystals, 10(4), 275. doi:10.3390/cryst10040275.

[19] Johnstone, R., & Thring, M. W. (1957). Pilot plants, models, and scale-up methods in chemical engineering. McGraw-Hill, New York, United States.

[20] Fernianti, D. (2000). Analysis of the reaction of solid CO_2 and $CaCO_3$ gases in a stirred tank slurry reactor. Ph.D. Thesis, Gadjah Mada University, Depok, Indonesia. (In Indonesian).

[21] Vasconcelos, J. M. T., Orvalho, S. P., & Alves, S. S. (2002). Gas-liquid mass transfer to single bubbles: Effect of surface contamination. AIChE Journal, 48(6), 1145–1154. doi:10.1002/aic.690480603.

[22] Fogler, H. S. (2010). Essentials of Chemical Reaction Engineering: Essenti Chemica Reactio Engi. Pearson Education, New York, United States.